Supplemental Information

Effects of Anthropogenic Emissions on Aerosol Formation from Isoprene and Monoterpenes in the Southeastern United States

Lu Xu[a], Hongyu Guo[b], Christopher M. Boyd[a], Mitchel Klein[c], Aikaterini Bougiatioti[b,d], Kate M. Cerully[a,1], James R. Hite[b], Gabriel Isaacman-VanWertz[e], Nathan M. Kreisberg[f], Christoph Knote[g], Kevin Olson[h], Abigail Koss[i,j], Allen H. Goldstein[e,h], Susanne V. Hering[f], Joost de Gouw[i,j], Karsten Baumann[k], Shan-Hu Lee[l], Athanasios Nenes[a,b,m], Rodney J. Weber[b], Nga Lee Ng[a,b,2]

[a]School of Chemical and Biomolecular Engineering, Georgia Institute of Technology, Atlanta, GA, USA

[b]School of Earth and Atmospheric Sciences, Georgia Institute of Technology, Atlanta, GA, USA

[c]Rollins School of Public Health, Emory University, Atlanta, GA, USA

[d]National Technical University of Athens, Laser Remote Sensing Laboratory, Zografou, Greece

[e]Department of Environmental Science, Policy and Management, University of California, Berkeley, CA, USA

[f]Aerosol Dynamics Inc., Berkeley, CA, USA

[g]Atmospheric Chemistry Division, National Center for Atmospheric Research, Boulder, CO, USA

[h]Department of Civil and Environmental Engineering, University of California, Berkeley, CA, USA

[i]NOAA Earth System Research Laboratory, Boulder, CO, USA

[j]Cooperative Institute for Research in Environmental Sciences, University of Colorado, Boulder, CO, USA

[k]Atmospheric Research and Analysis Inc., Morrisville, NC, USA

[l]Kent State University, College of Public Health, Kent, Ohio, USA

[m]Institute of Chemical Engineering Sciences (ICE-HT), Foundation for Research, Patras, Greece.

[1]Present address: TSI, Inc., Shoreview, MN, USA

[2]To whom correspondence may be addressed. Nga Lee Ng. Telephone Number: 404-385-2148. Address: 311 Ferst Drive NW, Atlanta, GA, 30332. E-mail: ng@chbe.gatech.edu

1. Field Campaign Description

1.1 Southern Oxidant and Aerosol Study (SOAS)

Measurements are performed at the SouthEast Aerosol Research and Characterization (SEARCH) site in Centreville, Alabama (32.94°N, 87.18°W) on June 1st – July 15th (2013) as part of the Southern Oxidant and Aerosol Study (SOAS) field campaign (http://soas2013.rutgers.edu/). A map of the southeastern US with the location of the Centreville site is shown in Fig. 2 in the main text. The sampling site is surrounded by forests and away from large urban areas (55km SE and 84 km SW of Tuscaloosa and Birmingham, AL, respectively). Isoprene is the dominant biogenic volatile organic compound (VOC) with a molar fraction of 82%, and there are also various monoterpenes such as α-pinene and β-pinene, which account for 8% and 7% of biogenic VOCs, respectively. Temperature during the sampling period typically peaks at 15:00 (28.6°C) and exhibits a minimum at 05:00 (21.6°C). Relative humidity is greater than 50% throughout the day and reaches ~90% at night. We define the nighttime as from 20:00 to 05:00 when the solar radiation is zero. Boundary layer height is measured by a ceilometer. The boundary layer height reaches a daily maximum (1300m) at about 17:00 and a daily minimum (375m) at about 07:00. The diurnal trends of temperature, relative humidity, and boundary layer height are shown in Fig. S1.

1.2 Southeastern Center for Air Pollution and Epidemiology (SCAPE)

In addition to SOAS, we conducted multiple ambient measurements in the greater Atlanta area as part of the Southeastern Center for Air Pollution and Epidemiology (SCAPE) study. SCAPE is an EPA-funded joint research project focusing on the study of air quality and the health effects of air pollutants. A map of the locations of the SCAPE sites is shown in the Fig. 2 in the main text. In our extensive field studies, four representative sites are chosen in the greater Atlanta area:

• Road-side site (RS, 33.775602 N, 84.390957 W): This site is on the Georgia Tech campus and only 5m away from Interstate 75/85.

• Georgia Tech site (GT, 33.779125 N, 84.395797 W): This site is located on the rooftop of the Ford Environmental Science & Technology Building at Georgia Tech, which is approximately 30-40m above ground and 840m away from the road-side site.

• Jefferson Street site (JST, 33.777501 N, 84.416667 W): This is a central SEARCH site that is located in Atlanta's urban area with a mixed commercial and residential neighborhood. It is about 2000m west of the Georgia Tech site.

• Yorkville site (YRK, 33.928528 N, 85.045483 W): This is a central SEARCH site located in a rural area at about 80km northwest of Jefferson Street site. This site, surrounded by agricultural land and forests, is characterized by large emissions of biogenic VOCs with occasional influence of anthropogenic emissions.

Our measurements in the greater Atlanta area were conducted from May 2012 to February 2013, with roughly one month at each site. Details about the sampling period at each site are listed in Table S1.

2. Instrumentation

The major relevant gas-phase and aerosol-phase instrumentations deployed in SOAS and SCAPE are described in more details in the following sections.

2.1 High-Resolution Time-of-Flight Aerosol Mass Spectrometer (HR-ToF-AMS)

An Aerodyne High-Resolution Time-of-Flight Aerosol Mass Spectrometer (HR-ToF-AMS) was deployed in both SOAS and SCAPE to measure the ambient non-refractory PM_1 (submicron particulate matter) composition. The working principles of the HR-ToF-AMS have been explained in detail elsewhere (1, 2). In brief, particles are sampled through an aerodynamic lens and then transmitted into a detection chamber where particles impact on a hot surface (600°C). Non-refractory species are flash evaporated and ionized with 70eV electron impact ionization. The ions generated are extracted into the time-of-flight mass spectrometer. Limited by the transmission efficiency of the aerodynamic lens, HR-ToF-AMS could only measure submicron aerosols. The time resolution of our HR-ToF-AMS measurements is set to be 2-3 minutes. The HR-ToF-AMS is operated in two optical modes (V or W) with different resolving power. W mode has higher resolving power (~4300 at *m/z* 200) than V mode (~2100 at *m/z* 200), but the sensitivity of W mode is lower than V mode. Considering the mass concentration in this study, only V mode data are reported. Ambient filter measurements (with a particle filter placed upstream of the instrument) are performed periodically on a daily base in order to correct gas-phase interference on the particle signals measured by the HR-ToF-AMS. Ionization efficiency

(IE) calibrations are conducted every week and the variation in Airbeam/IE is within 20%. A nafion dryer is placed upstream of the HR-ToF-AMS to ensure that the relative humidity is below 20% to eliminate potential relative humidity effect on particle collection efficiency (CE) at the vaporizer. Composition-dependent CE is applied given the presence of large amount of sulfate (3). The data analysis is performed using the standard AMS analysis toolkits SQUIRREL v1.53 and PIKA v1.12 in Igor Pro 6.34 (WaveMetrics Inc.). The time series, diurnal trend of non-refractory species (organics, sulfate, nitrate, ammonium, and chloride) in Centreville, and normalized mass spectrum of organics as quantified by HR-ToF-AMS are shown in Fig. S2.

2.2 Particle Into Liquid Sampler - Ion Chromatograph system (PILS-IC); Particle Into Liquid Sampler - Liquid Waveguide Capillary Cell - Total Organic Carbon analyzer (PILS-LWCC-TOC)

A Particle Into Liquid Sampler (PILS) is coupled to Ion Chromatograph (IC) to measure the concentration of water-soluble inorganic compounds (4) in SOAS. From June 1st to June 23rd 2013, a $PM_{2.5}$ cyclone is placed upstream of the PILS-IC. On June 24th, we replaced the $PM_{2.5}$ cyclone with a PM_1 cyclone. To be consistent with the particle size range detected by HR-ToF-AMS (i.e., PM_1), only PILS-IC data after June 24th 2013 are reported in this study.

A second PILS is coupled to a Liquid Waveguide Capillary Cell - Total Organic Carbon analyzer (LWCC-TOC) system to continuously measure the concentration of water-soluble brown carbon. Detailed description of this instrument can be found in Hecobian et al. (5). Briefly, PILS dissolves water-soluble species from the sample flow and the liquid sample coming out of the PILS is continuously injected into a Liquid Waveguide Capillary Cell via a syringe pump. Absorption spectra are collected over a range of wavelengths (200-800 nm), based on which the absorption of water soluble carbon at 365nm is calculated.

2.3 Thermal Desorption Aerosol Gas Chromatography Instrument (TAG)

Particle-phase concentrations of 2-methylerythritol and 2-methylthreitol (collectively referred to as methyltetrols) and levoglucosan are measured hourly using a Semi-Volatile Thermal desorption Aerosol Gas chromatograph (SV-TAG), modified to include in-situ derivatization of oxygenated tracers. This instrument is described in detail by Isaacman et al. (6). Briefly, sample is collected at 10 SLPM into two parallel custom collection and thermal desorption cells, each consisting of a high surface area metal fiber filter in a custom thermally

controlled stainless steel housing that quantitatively collects particle- and gas-phase compounds with a vapor pressure as high as tetradecane (7). Sample collected in one of the two cells is passed through a 16-inch-long multi-channel carbon monolith (MAST carbon: 500 channel, 30 mm diameter) to remove all gas-phase compounds, while a simultaneous unperturbed sample is collected in the other cell. Though total gas-plus-particle-phase concentrations and direct measurements of fraction in the particle phase are also accessible using these parallel cells, only particle-phase concentrations are used for comparisons in this work to allow direct comparison to PMF factors from HR-ToF-AMS data.

Samples are transferred from the collection cell to the head of a gas chromatography column in a two-step thermal desorption cycle with a temperature ramp from 30°C to 315°C and an intermediate purge-and-trap on a custom pre-concentration trap as described by Zhao et al. (7). Desorption helium is saturated with a silylating agent, converting hydroxyl groups, which cannot be effectively analyzed by gas chromatography, into less-polar trimethylsilyl esters and ethers. Compounds are separated and analyzed with a non-polar chromatography column (Rxi-5Sil MS: 20m x 0.15 mm x 0.15 μm; Restek Corporation) in a custom-modified gas chromatograph/mass spectrometer (7890/5975C; Agilent Technologies). Collection cells are isolated from the gas chromatograph using a custom valveless interface (8) to allow simultaneous sample collection and analysis, allowing hourly time resolution (with 22 minutes of sample collection in each hour, under typical operating conditions).

2.4 Gas Chromatography - Mass Spectrometry (GC-MS)

Volatile organic compounds (VOCs) having 1 to 12 carbon atoms (C_1-C_{12}) are measured by gas-chromatography mass-spectrometry (GC-MS) (9). The detection limit, precision, and accuracy vary slightly between compounds but are generally about 10pptv, 15%, and 25%, respectively. The inlet for the GC-MS consists of an unheated 30m Teflon line and samples from approximately 20m above ground level. Ambient air is pumped through the inlet at approximately 5 SLPM. Two smaller streams (Channel 1 and Channel 2) of 70 sccm each are subsampled horizontally off the main inlet. Channel 1 analyzes C_2-C_5 hydrocarbons. Channel 2 analyzes C_5-C_{12} hydrocarbons and hetero-atom containing compounds. Channel 1 sample passes through a trap consisting of Ascarite (Thomas Scientific) to remove water and CO_2. Channel 2 sample passes through a trap containing granular Na_2SO_3 (Fisher Scientific) to remove ozone.

Both sample streams then pass through a cryogenically cooled (-35°C) trap to further remove water. Sample streams are then directed into cryogenic traps at -165°C for five minutes every half hour. After the five minute sampling period, the Channel 1 cryogenic trap is flash heated from -165°C to 100°C. The sample is briefly cryofocused then injected onto an 18m Al_2O_3/KCl PLOT column, which is ramped from 55°C to 150°C in 3.5 minutes. The Channel 2 cryogenic trap is then flash heated and sample is injected onto a 20m DB-624 column, which is ramped from 38°C to 130°C in 11 minutes. Column eluent is ionized with electron ionization (EI) and analyzed by a linear quadrupole mass spectrometer (Agilent 5973) operating in selected ion mode.

3. Positive Matrix Factorization (PMF)

Positive Matrix Factorization (PMF) (10, 11) is a multivariate factor analysis technique. PMF analysis represents the observed data as the linear combination of a number of factors with constant source profiles (mass spectrum for HR-ToF-AMS data) but varying concentration contributions across the dataset. Specifically, PMF solves the bilinear factor model

$$x_{ij} = \sum_p g_{ip} f_{pj} + e_{ij} \quad \text{Eqn 1}$$

where x_{ij} is the measured values of j species in i sample, p is the number of factors, f_{pj} is the fraction of j species in the source profile of certain factor, g_{ip} is the contribution of certain factor in i sample, e_{ij} is the residual of j species in i sample, by minimizing the summed least squares errors of the fit weighted with the error estimates of each sample. PMF analysis requires no priori assumption and constrains solution to have non-negative values, which provides more physically meaningful solutions than other receptor models.

PMF analysis is performed on high-resolution mass spectra of organic species (nitrate and sulfate functional groups are not included) for source apportionments. Organic data matrix and error matrix are generated from PIKA v1.12. The PMF Evaluation Toolkit (PET) software is utilized to process the data (12). Any "weak" *m/z*'s (whose signal-to-noise ratio ranges between 0.2 and 2) are downweighted by a factor of 2, and "bad" *m/z*'s (whose signal-to-noise ratio is smaller than 0.2) are removed to reduce disproportionate effects on the results (13). Four organic ions (O^+, HO^+, H_2O^+, and CO^+), which are scaled to CO_2^+ in PIKA v1.12, are downweighted prior to PMF analysis to avoid excessive weighting of CO_2^+. The error of CHO^+ (*m/z* 29.0027) is

downweighted by a factor of 4 as its error appears to be underestimated, possibly due to interference from its adjacent N_2 isotope ion (*m/z* 29.0032). PMF solutions for Centreville and all SCAPE datasets are evaluated by following the detailed procedure listed in Zhang et al. (14). For simplicity, we only show the key diagnostic plots of the PMF results for the Centreville data in Fig. S3.

For the Centreville data, a 4-factor solution is chosen after carefully checking the quality of the fit parameter (Q/Q_{exp}). Solutions with more than 4 factors display splitting behavior of existing factors instead of providing new factors (12). The rotational ambiguity of the 4-factor solution is examined by varying the FPEAK parameter. We do not find improved correlations with external tracers for FPEAK values that are different from 0. Therefore, a FPEAK value of 0 is selected for the solution. For the 4-factor solution with FPEAK=0, the scaled residual of each *m/z* is relatively uniformly distributed (panel (e) in Fig. S3) and the reconstructed organic aerosol concentration agrees well with measurement (panel (f) in Fig.S3). Combing the key diagnostic plots and PMF solutions with characteristic mass spectral signature, diurnal pattern, and correlation with external tracers (shown in the main text), we find the 4-factor solution with FPEAK=0 to be the most reasonable and meaningful solution.

Various factors are identified in Centreville and SCAPE datasets. In this study, we focus on the effects of anthropogenic emissions on biogenic SOA, including the isoprene-derived OA (Isoprene-OA) and less-oxidized oxygenated OA (LO-OOA). The identification of Isoprene-OA, LO-OOA, more-oxidized oxygenated organic aerosol (MO-OOA), and biomass burning OA (BBOA) are discussed in the main text. It is important to note that the BBOA and Isoprene-OA reported in this study likely only represent fresh OA from biomass burning and isoprene oxidation, respectively. Recent laboratory studies (15, 16) revealed that the oxidation of levoglucosan is fast in both gas phase and aqueous phase. The fast oxidation of levoglucosan can result in the rapid decay of signals at $C_2H_4O_2^+$ (*m/z* 60) and $C_3H_5O_2^+$ (*m/z* 73), causing the mass spectrum of BBOA to resemble that of MO-OOA (17). Thus, the aged OA from biomass burning could be apportioned to MO-OOA factor. It is possible that Isoprene-OA would lose its signature ($C_4H_5^+$ and $C_5H_6O^+$) in the mass spectrum during aging as well, though currently there are no data reported in terms of how fast this process occurs in the atmosphere. Taken together, the

mass fractions of the BBOA and Isoprene-OA factors likely serve as a lower bound of OA from biomass burning and isoprene photooxidation.

Here, we briefly discuss the identification of cooking OA (COA) and hydrocarbon-like OA (HOA), which are also important OA sources for several datasets shown in Fig.2. Hydrocarbon-like organic aerosol (HOA) is a surrogate of primary OA from vehicle emissions (14). Among all the OA factors, HOA is the least oxidized and its mass spectrum is dominant by hydrocarbon-like ions ($C_xH_y^+$ ions), which is similar to the mass spectrum of primary combustion emission species (14). In addition, HOA is only identified in urban sites (Roadside site, Georgia Tech site, and Jefferson Street site), which is consistent with the lower anthropogenic emissions in rural sites. HOA shows clear diurnal pattern with evident morning and evening rush hour peaks.

Cooking OA (COA) is identified in urban sites throughout the year. The mass spectrum of this factor is characterized by prominent signal at ion $C_3H_5^+$ (*m/z* 41) and $C_4H_7^+$ (*m/z* 55), which is similar to the mass spectrum of unsaturated fatty acids (18, 19). COA has a clear and unique diurnal trend, which shows a small peak at lunch time and a large peak at dinner time. In addition to Atlanta, the COA factor has also been detected in megacities all over the world (18, 20-22), indicating cooking is an important source for OA in urban areas.

Elemental ratios (O:C, H:C, N:C, and OM:OC) of PMF factors are determined by following the procedure in Canagaratna et al. (23). Since nitrate functional groups (NO^+ and NO_2^+ ions) of organic compounds are excluded in PMF analysis, NO^+ and NO_2^+ ion are not included in N:C calculation.

4. Multivariate Linear Regression

Our multivariate linear regression equation takes the following form:

$$[\text{Isoprene-OA}] = \beta_0 + \beta_1 \times [H_2O_{ptcl}] + \beta_2 \times H^+_{(aq)} + \beta_3 \times [SO_4^{2-}] + \sum_{i=0}^{23} \alpha_i \times \text{hour}_i \qquad \text{Eqn 2}$$

The dependent variable is the concentration of Isoprene-OA factor and the explanatory variables are particle water content ($[H_2O_{ptcl}]$, μg m^{-3} air), particle acidity ($H^+_{(aq)}$, mol L^{-1} H_2O), sulfate ($[SO_4^{2-}]$, μg m^{-3} air) as well as 24 hour-of-day indicator variables capturing the diurnal variation

of Isoprene-OA. The 24 hour-of-day indicator variables are included in this regression analysis in order to account for the diurnal variation of Isoprene-OA. For example, the interpretation of β-coefficient of sulfate is the effect of sulfate on Isoprene-OA at the same hour of day and holding $[H_2O_{ptcl}]$ and $H^+_{(aq)}$ constant. If the indicator variables are not included, we cannot rule out the possibility that the association between Isoprene-OA and sulfate is caused by the fact that they have similar diurnal trends.

Details regarding the calculation and uncertainty of particle water content and particle acidity can be found in Guo et al. (24). Briefly, we calculate the particle water content by including water uptake by both inorganics and organics. Water uptake by inorganics is calculated from the thermodynamic model ISORROPIA II (25) by including SO_4^{2-}, NH_4^+, NO_3^-, Cl^-, Na^+, Ca^{2+}, Mg^{2+}, and K^+ as well as gas-phase NH_3. In Centreville, the concentrations of all inorganic ions are from PILS-IC measurements. In SCAPE datasets, only SO_4^{2-}, NH_4^+, NO_3^- and Cl^- are included and they are from HR-ToF-AMS measurements, since PILS-IC was not deployed in the SCAPE study. Water uptake by organics is calculated based on the measured concentration and hygroscopicity of organics. Organic concentration is measured by the HR-ToF-AMS. Organic hygroscopicity is inferred from total measured hygroscopicity via Cloud Condensation Nuclei counter (CCN) by subtracting the contribution from inorganic species (26). Water uptake by organics contributes to 36% of total water in SOAS. The calculated $[H_2O_{ptcl}]$ agrees with our indirect measurements of particle water content (24). Further, particle acidity ($H^+_{(aq)}$, mol L^{-1} H_2O) is calculated based on $[H_2O_{ptcl}]$ and output $[H^+]$ (μg m^{-3} air) from ISORROPIA II. The ISORROPIA equilibrium calculations accurately predict the measured gas-phase ammonia concentration (24), providing strong validation for our particle acidity calculation.

We use SAS (version 9.4; SAS Institute Inc., Cary, NC) for all of our statistical analyses. For the Centreville data, a total of 615 data points (one hour average data) are included in the model. The significance of the 24 indicator variables is tested as a group. We find a statistically significant ($p=0.0001$) positive linear relationship between indicator variables and Isoprene-OA, indicating that the indicator variables can capture the diurnal variation of Isoprene-OA.

5. Effects of Particle Water (H_2O_{ptcl}), Particle Acidity (H^+), and Sulfate (SO_4^{2-}) on Isoprene-OA Factor for SCAPE Datasets

Fig. S6 shows $H^+_{(aq)}$ (mol L^{-1} H_2O) as a function of [H_2O_{ptcl}] (μg m^{-3} air) for Centreville, Jefferson Street (JST_May), Yorkville (YRK_July), and Georgia Tech (GT_Aug), where the Isoprene-OA factor is resolved. For each site, all data points are grouped into nine subplots based on sulfate concentration. An increment of 0.5, 0.5, 0.8, and 0.8 μg m^{-3} in [SO_4^{2-}] is chosen for Centreville, JST_May, YRK_July, and GT_Aug, respectively, in order to evenly distribute the data points into nine subplots. The size of data points represents the concentration of Isoprene-OA. The maximum concentration of the Isoprene-OA factor is 5.3, 1.9, 11.1, 6.9 μg m^{-3} for Centreville, JST_May, YRK_July, and GT_Aug, respectively.

As mentioned in the Fig. 3B of main text, a range of $H^+_{(aq)}$ is observed for the same [H_2O_{ptcl}] in Centreville, which is likely due to difference in gas-phase [NH_3]. As shown in Fig. S6(a), $H^+_{(aq)}$ is lower when gas-phase [NH_3] is higher under similar [H_2O_{ptcl}]. In contrast, only a narrow range of $H^+_{(aq)}$ is obtained for the same [H_2O_{ptcl}] in SCAPE datasets because [NH_3] data are not available and thus not included in the $H^+_{(aq)}$ calculation.

6. Backtrajectory Analysis

Backtrajectories have been calculated every 3 hours with the Lagrangian particle dispersion model (FLEXPART) (27) in version 9.02 (http://flexpart.eu) using 6-hourly meteorological analysis data of the Global Forecasting System (GFS) of the National Centers for Environmental Prediction (NCEP) (http://nomads.ncep.noaa.gov/txt_descriptions/GFS_half_degree_doc.shtml), interlaced with 3 hour forecasts (0, 3, 6, 9, 12, 15, 18, 21 UTC), at a horizontal resolution of 0.5°. 400,000 particles are released randomly within the first three hours of a simulation from the location of the Centreville site and followed back in time for 72 hours. We here consider 'particle' to refer to an infinitesimally small parcel of air, an inert 'air mass tracer', that is only affected by three-dimensional transport, turbulence and convection, but does not have any removal processes (no deposition, sedimentation, or chemical loss). Particle residence times, i.e., the concentration of particles times the time spent in a given grid cell, are then integrated over the simulation period to derive fractional contributions of each sector to the air mass history.

To examine if the diurnal trend of LO-OOA in Centreville varies with different origins of air mass, we split the field into four quadrants relative to the measurement location of Centreville: northwesterly (NW), northeasterly (NE), southwesterly (SW), and southeasterly (SE). Then we assign each backtrajectory (3hr period) an origin based on the quadrant with the largest residence time. For example, if 60% of one backtrajectory stays in the northwestern quadrant, we assign this backtrajectory to NW. Following this procedure, 348 backtrajectories are assigned into four groups: NW (156), NE (21), SW (120), SE (51). Fig. S9 shows the integrated backtrajectory residence time of four quadrants. Further, the LO-OOA data (time step = 2-3 min) are averaged into 3hr time resolution in order to match the time step of the backtrajectory. According to the origin of the corresponding backtrajectory, LO-OOA is also categorized into four groups. Fig. S10 (a) shows the grouped diurnal trend of LO-OOA based on the origin of the air masses. LO-OOA concentration is higher at night than in the day regardless of the origins of the air masses, indicating that LO-OOA has a local source. We note that when the air mass comes from the NE and SE, the LO-OOA diurnal trend shows a relatively larger variability due to lower frequency of air mass originating from these two quadrants.

The same backtrajectory analysis has also been performed for Isoprene-OA factor. Isoprene-OA also shows a similar diurnal pattern (peaks in late afternoon) regardless of the origins of the air masses as shown in Fig. S10(c). This suggests that the source of Isoprene-OA is local.

7. Organic Nitrate Estimation

The mass concentration of the nitrate functional groups (-ONO_2 subunit) in organic compounds is estimated based on the difference between HR-ToF-AMS measurements and PILS-IC measurements (4). While PILS-IC measures –ONO_2 from inorganic nitrate only, HR-ToF-AMS could measure –ONO_2 from both organic and inorganic nitrates. Unlike PILS-IC, which directly measures the concentration of –ONO_2 subunit, HR-ToF-AMS has extensive fragmentation caused by strong electron impact ionization. Thus, -ONO_2 subunit appears mostly as NO_x^+ ions (NO^+ and NO_2^+) in HR-ToF-AMS (28). In this study, we use the concentration of NO^+ and NO_2^+ to estimate the concentration of –ONO_2 for HR-ToF-AMS following Eqn 3, in which 30, 46, and 62 are the molecular weights of NO^+, NO_2^+, and -ONO_2, respectively.

$$[\text{-ONO}_2]_{AMS}=[NO^+]\times\frac{62}{30}+[NO_2^+]\times\frac{62}{46} \quad \text{Eqn 3}$$

The mass concentration of nitrate functional groups in organic compounds ($[\text{-ONO}_2]_{Org}$) is used to estimate the mass concentration of organic nitrates according to Eqn 4. MW_{ON} is the average molecular weight of organic nitrates, which is assumed to range from 200 to 300 g mol^{-1} according to Rollins et al. (29). Fig. S11. shows the diurnal trends of organic nitrates contribution to LO-OOA.

$$[ON]=\frac{[\text{-ONO}_2]_{org}}{62}\times MW_{ON} \quad \text{Eqn 4}$$

8. [$NO_3^{\bullet}$] Estimation

In SOAS, the reactive loss of $NO_3^{\bullet}$ is much larger than the sinks of N_2O_5 (homogeneous reaction with water and heterogeneous uptake to particles) as shown below.

The $NO_3^{\bullet}$ lifetime with respect to reaction with biogenic VOCs ($\tau_{NO3,\,BVOCs}$) is

$$\tau_{NO3,BVOCs}=\frac{1}{\sum k_i[VOC_i]}$$

In Centreville, a suite of VOCs is measured with Gas-Chromatography Mass-Spectrometer (GC-MS). Using the campaign-average nighttime concentrations of the VOCs and the reaction rate constants of VOCs+$NO_3^{\bullet}$ at typical nighttime temperature (25°C), as listed in Table S3, results in a $\tau_{NO3,BVOCs}$ value of 8s.

The N_2O_5 lifetime with respect to heterogeneous uptake onto aqueous particles ($\tau_{N2O5,het}$) is

$$\tau_{N2O5,het}=\frac{1}{k_{het}},$$

in which k_{het} is the rate for heterogeneous uptake. According to Fry et al. (30),

$$k_{het}=\frac{\gamma\nu}{4}SA,$$

in which γ is the uptake coefficient, ν is the molecular speed, and SA is the surface area of particles. By using 1) γ = 0.045 (upper limit for N_2O_5 uptake to particle with different composition according to Gaston et al. (31)); 2) ν = $2.3*10^4$ cm s^{-1} according to Fry et al. (30); and 3) average SA = 200 μm^2 cm^{-3}, we calculate that $\tau_{N2O5,het}$ is about 1900s.

The N_2O_5 lifetime with respect to reaction with H_2O ($\tau_{N2O5,H2O}$) according to Crowley et al. (32) is

$$\tau_{N2O5,H2O} = \frac{1}{k_{H_2O}} = \frac{1}{2.5\times10^{-22}[H_2O] + 1.8\times10^{-39}[H_2O]^2},$$

in which k_{H2O} is the reaction rate of N_2O_5 and H_2O, $[H_2O]$ is the water concentration in the unit of molecule cm^{-3}. $[H_2O]$ reaches a daily maximum of ~10 μg m^{-3} (~$3.3*10^{11}$ molecule cm^{-3}) at around 7am. Using $[H_2O]$ = ~$3.3*10^{11}$ molecule cm^{-3} results in a $\tau_{N2O5,H2O}$ value of $1.2*10^{10}$ s.

In conclusion, the lifetime of $NO_3^\bullet$ with respect to reaction with BVOCs (8s) is much shorter than the lifetime of N_2O_5 with respect to heterogeneous uptake (1900s) and homogeneous reaction with H_2O ($1.2*10^{10}$s).

Therefore, we could estimate $[NO_3^\bullet]$ based on that the production mechanism for $NO_3^\bullet$ at night is the reaction of NO_2 with O_3 and the major loss mechanism for $NO_3^\bullet$ is its reaction with VOCs (Eqn 5).

$$\frac{d[NO_3^\bullet]}{dt} = k_1[O_3]\times[NO_2] - (\sum k_i[VOC_i])\times[NO_3^\bullet] \qquad \text{Eqn 5}$$

Due to the estimated high reactivity of $NO_3^\bullet$ (8s), we can assume $NO_3^\bullet$ is at steady state. With this, we can express $[NO_3^\bullet]$ as:

$$[NO_3^\bullet] = \frac{k_1[O_3][NO_2]}{\sum k_i[VOC_i]} \qquad \text{Eqn 6}$$

The average nighttime $[O_3]$ and $[NO_2]$ are 21ppb and 0.54ppb, respectively. Using the concentration of each species and $k_1=3.52\times10^{-17}$ cm^3 $molec^{-1}$ s^{-1} (from Master Chemical

Mechanism via website http://mcm.leeds.ac.uk/MCM/, under 25°C) (33), the [$NO_3^\bullet$] is calculated to be 7.6×10^{-2} ppt.

9. Laboratory Chamber Experiments

The secondary organic aerosol (SOA) yields from β-pinene oxidation by $NO_3^\bullet$ radical under similar conditions (mass loading, temperature, relative humidity, aerosol acidity, and RO_2 fate) as Centreville are measured in the Georgia Tech Environmental Chamber facility (GTEC). Prior to each experiment, the 12 m^3 Teflon chambers are continuously flushed for 24 hours with purified air (AADCO pure air generator). All experiments are conducted at 25°C. NO_2 and O_3 are injected separately and then mixed in the chamber. The reaction of NO_2 with O_3 could form $NO_3^\bullet$ through the reaction R1. NO_2 and O_3 concentrations are chosen ([NO_2]:[O_3] ≈ 4:3, molar ratio) to ensure that 99% of the β-pinene is oxidized by $NO_3^\bullet$ instead of ozone. In order to ensure that the majority of $RO_2^\bullet$ reacts with $HO_2^\bullet$ instead of $RO_2^\bullet$, which is likely the fate of $RO_2^\bullet$ at night in the southeastern US (34), formaldehyde is injected into chamber by passing pure air over formalin solution (Sigma-Aldrich, 37% HCHO) in a glass bulb. The reaction of formaldehyde and $NO_3^\bullet$ can generate $HO_2^\bullet$ through the reaction R2. A systematic set of experiments is carried out for a range of initial β-pinene mixing ratios (3-15ppb) under both dry (RH<2%) and humid (RH ~70%) conditions with acidic seed particles (ammonium sulfate/sulfuric acid mixture, $(NH_4)_2SO_4$:H_2SO_4 = 3:5, molar ratio).

$$NO_2 + O_3 \rightarrow NO_3 + O_2 \qquad \text{R1}$$

$$HCHO + NO_3^\bullet + O_2 \rightarrow HNO_3 + CO + HO_2^\bullet \qquad \text{R2}$$

High Resolution Time-of-Flight Aerosol Mass Spectrometer (HR-ToF-AMS) and Scanning Mobility Particle Sizer (SMPS) are used to characterize aerosol growth and particle-phase composition. The gas-phase compositions are monitored with Chemical Ionization Mass Spectrometer (CIMS), ozone, and NO_x monitors. The SOA yield is found to range from 0.32 to 0.64, which depends on aerosol mass loading. Specifically, the SOA yield under conditions that are similar to Centreville (i.e., mass loading, temperature, relative humidity, aerosol acidity, and RO_2 fate) is 0.50.

10. Estimation of Contributions from Different VOCs to LO-OOA

To provide observational constraints on the contribution of $NO_3^{\bullet}$ chemistry to LO-OOA, we estimate aerosol formation from isoprene, α-pinene, and β-pinene, which are the most abundant SOA precursors measured in Centreville, via various oxidation pathways. At night, the main oxidants are $NO_3^{\bullet}$ radicals and ozone. Based on the oxidant concentration (measured $[O_3]$ 21ppb and estimated $[NO_3^{\bullet}]$ 7.6×10^{-2} ppt) and the reaction rate constant of each BVOC with O_3 and $NO_3^{\bullet}$, we can estimate the branching ratio of each BVOC that reacts with $NO_3^{\bullet}$ (Eqn 7). We calculate that 17%, 20%, and 38% of isoprene, α-pinene, and β-pinene, respectively, reacts with $NO_3^{\bullet}$ at night (Table S5).

$$\text{branching ratio}_{\text{species i}+NO_3^{\bullet}} = \frac{k_{[\text{species i} + NO_3]} \times [NO_3^{\bullet}]}{k_{[\text{species i} + NO_3]} \times [NO_3^{\bullet}] + k_{[\text{species i} + O_3]} \times [O_3]} \quad \text{Eqn 7}$$

$$[\text{SOA}]_{\text{species,oxidant}} = [\text{species}] \bullet \text{branching ratio}_{\text{species,oxidant}} \bullet \text{yield}_{\text{species,oxidant}} \quad \text{Eqn 8}$$

Combining the estimated branching ratio and SOA yield from chamber studies (Eqn 8), we calculate that 0.7 μg m^{-3} of SOA would be produced (Table S5), which agrees within a factor of three with measured nighttime LO-OOA production (1.7 μg m^{-3} from 17:00 to sunrise). Fig. S12 illustrates our estimated contribution from different oxidation pathway and different VOCs to nighttime OA production. SOA from biogenic VOCs+$NO_3^{\bullet}$ accounts for about 64% of total nighttime OA production. Specifically, β-pinene+$NO_3^{\bullet}$ accounts for 80% of OA from the $NO_3^{\bullet}$ oxidation pathway, which corresponds to about 50% of total nighttime OA production.

References

1. Canagaratna MR*, et al.* (2007) Chemical and microphysical characterization of ambient aerosols with the aerodyne aerosol mass spectrometer. *Mass Spectrometry Reviews* 26(2):185-222.
2. DeCarlo PF*, et al.* (2006) Field-Deployable, High-Resolution, Time-of-Flight Aerosol Mass Spectrometer. *Anal Chem* 78(24):8281-8289.
3. Middlebrook AM, Bahreini R, Jimenez JL, & Canagaratna MR (2012) Evaluation of Composition-Dependent Collection Efficiencies for the Aerodyne Aerosol Mass Spectrometer using Field Data. *Aerosol Sci Tech* 46(3):258-271.
4. Orsini DA*, et al.* (2003) Refinements to the particle-into-liquid sampler (PILS) for ground and airborne measurements of water soluble aerosol composition. *Atmospheric Environment* 37(9-10):1243-1259.
5. Hecobian A*, et al.* (2010) Water-Soluble Organic Aerosol material and the light-absorption characteristics of aqueous extracts measured over the Southeastern United States. *Atmos. Chem. Phys.* 10(13):5965-5977.
6. Isaacman G*, et al.* (2014) On-line derivatization for hourly measurements of gas- and particle-phase Semi-Volatile oxygenated organic compounds by Thermal desorption Aerosol Gas chromatography (SV-TAG). *Atmos. Meas. Tech. Discuss.* 7(7):7495-7529.
7. Zhao Y*, et al.* (2012) Development of an In Situ Thermal Desorption Gas Chromatography Instrument for Quantifying Atmospheric Semi-Volatile Organic Compounds. *Aerosol Sci Tech* 47(3):258-266.
8. Kreisberg NM*, et al.* (2014) Development of an automated high temperature valveless injection system for on-line gas chromatography. *Atmos. Meas. Tech. Discuss.* 7(7):7531-7567.
9. Gilman JB*, et al.* (2010) Ozone variability and halogen oxidation within the Arctic and sub-Arctic springtime boundary layer. *Atmos. Chem. Phys.* 10(21):10223-10236.
10. Paatero P & Tapper U (1994) Positive Matrix Factorization - a Nonnegative Factor Model with Optimal Utilization of Error-Estimates of Data Values. *Environmetrics* 5(2):111-126.
11. Paatero P (1997) A weighted non-negative least squares algorithm for three-way 'PARAFAC' factor analysis. *Chemometr Intell Lab* 38(2):223-242.
12. Ulbrich IM, Canagaratna MR, Zhang Q, Worsnop DR, & Jimenez JL (2009) Interpretation of organic components from Positive Matrix Factorization of aerosol mass spectrometric data. *Atmos. Chem. Phys.* 9(9):2891-2918.
13. Ulbrich IM, Canagaratna MR, Zhang Q, Worsnop DR, & Jimenez JL (2009) Interpretation of organic components from Positive Matrix Factorization of aerosol mass spectrometric data. *Atmos. Chem. Phys.* 9(9):2891-2918.
14. Zhang Q*, et al.* (2011) Understanding atmospheric organic aerosols via factor analysis of aerosol mass spectrometry: a review. *Anal Bioanal Chem* 401(10):3045-3067.
15. May AA, Saleh R, Hennigan CJ, Donahue NM, & Robinson AL (2012) Volatility of Organic Molecular Markers Used for Source Apportionment Analysis: Measurements and Implications for Atmospheric Lifetime. *Environ Sci Technol* 46(22):12435-12444.
16. Zhao R, Mungall EL, Lee AKY, Aljawhary D, & Abbatt JPD (2014) Aqueous-phase photooxidation of levoglucosan – a mechanistic study using aerosol time-of-flight chemical ionization mass spectrometry (Aerosol ToF-CIMS). *Atmos. Chem. Phys.* 14(18):9695-9706.
17. Bougiatioti A*, et al.* (2014) Processing of biomass-burning aerosol in the eastern Mediterranean during summertime. *Atmos. Chem. Phys.* 14(9):4793-4807.

18. Huang XF*, et al.* (2010) Highly time-resolved chemical characterization of atmospheric submicron particles during 2008 Beijing Olympic Games using an Aerodyne High-Resolution Aerosol Mass Spectrometer. *Atmos Chem Phys* 10(18):8933-8945.
19. Mohr C*, et al.* (2009) Characterization of Primary Organic Aerosol Emissions from Meat Cooking, Trash Burning, and Motor Vehicles with High-Resolution Aerosol Mass Spectrometry and Comparison with Ambient and Chamber Observations. *Environ Sci Technol* 43(7):2443-2449.
20. Robinson AL, Subramanian R, Donahue NM, Bernardo-Bricker A, & Rogge WF (2006) Source Apportionment of Molecular Markers and Organic Aerosol. 3. Food Cooking Emissions. *Environ Sci Technol* 40(24):7820-7827.
21. Crippa M*, et al.* (2013) Wintertime aerosol chemical composition and source apportionment of the organic fraction in the metropolitan area of Paris. *Atmos. Chem. Phys.* 13(2):961-981.
22. Crippa M*, et al.* (2014) Organic aerosol components derived from 25 AMS data sets across Europe using a consistent ME-2 based source apportionment approach. *Atmos. Chem. Phys.* 14(12):6159-6176.
23. Canagaratna MR*, et al.* (2014) Elemental ratio measurements of organic compounds using aerosol mass spectrometry: characterization, improved calibration, and implications. *Atmos. Chem. Phys. Discuss.* 14(13):19791-19835.
24. Guo H*, et al.* (2014) Particle water and pH in the southeastern United States. *Atmos. Chem. Phys. Discuss.* 14(19):27143-27193.
25. Fountoukis C & Nenes A (2007) ISORROPIA II: a computationally efficient thermodynamic equilibrium model for K+-Ca2+-Mg2+-NH(4)(+)-Na+-SO42--NO3--Cl--H2O aerosols. *Atmos Chem Phys* 7(17):4639-4659.
26. Cerully K*, et al.* (2014) On the Link Between Hygroscopicity, Volatility, and Oxidation State of Ambient and Water-soluble Aerosol in the Southeastern United States. *Atmos. Chem. Phys. Discuss.* 14, 2014.
27. Stohl A, Forster C, Frank A, Seibert P, & Wotawa G (2005) Technical note: The Lagrangian particle dispersion model FLEXPART version 6.2. *Atmos. Chem. Phys.* 5(9):2461-2474.
28. Farmer DK*, et al.* (2010) Response of an aerosol mass spectrometer to organonitrates and organosulfates and implications for atmospheric chemistry. *P Natl Acad Sci USA* 107(15):6670-6675.
29. Rollins AW*, et al.* (2012) Evidence for NOx Control over Nighttime SOA Formation. *Science* 337(6099):1210-1212.
30. Fry JL*, et al.* (2013) Observations of gas- and aerosol-phase organic nitrates at BEACHON-RoMBAS 2011. *Atmos Chem Phys* 13(17):8585-8605.
31. Gaston CJ, Thornton JA, & Ng NL (2014) Reactive uptake of N2O5 to internally mixed inorganic and organic particles: the role of organic carbon oxidation state and inferred organic phase separations. *Atmos. Chem. Phys.* 14(11):5693-5707.
32. Crowley JN*, et al.* (2011) Variable lifetimes and loss mechanisms for NO3 and N2O5 during the DOMINO campaign: contrasts between marine, urban and continental air. *Atmos Chem Phys* 11(21):10853-10870.
33. Saunders SM, Jenkin ME, Derwent RG, & Pilling MJ (2003) Protocol for the development of the Master Chemical Mechanism, MCM v3 (Part A): tropospheric degradation of non-aromatic volatile organic compounds. *Atmos Chem Phys* 3:161-180.
34. Mao J*, et al.* (2012) Insights into hydroxyl measurements and atmospheric oxidation in a California forest. *Atmos. Chem. Phys.* 12(17):8009-8020.
35. Ng NL*, et al.* (2008) Secondary organic aerosol (SOA) formation from reaction of isoprene with nitrate radicals (NO(3)). *Atmos Chem Phys* 8(14):4117-4140.

36. Kleindienst TE, Lewandowski M, Offenberg JH, Jaoui M, & Edney EO (2007) Ozone-isoprene reaction: Re-examination of the formation of secondary organic aerosol. *Geophysical Research Letters* 34(1).
37. Hallquist M, Wängberg I, Ljungström E, Barnes I, & Becker K-H (1999) Aerosol and Product Yields from NO3 Radical-Initiated Oxidation of Selected Monoterpenes. *Environ Sci Technol* 33(4):553-559.
38. Shilling JE*, et al.* (2008) Particle mass yield in secondary organic aerosol formed by the dark ozonolysis of alpha-pinene. *Atmos Chem Phys* 8(7):2073-2088.
39. Griffin RJ, Cocker DR, Flagan RC, & Seinfeld JH (1999) Organic aerosol formation from the oxidation of biogenic hydrocarbons. *J Geophys Res-Atmos* 104(D3):3555-3567.

Table S1. Sampling sites and periods for the Southeastern Center of Air Pollution and Epidemiology (SCAPE) study and the Southern Oxidant and Aerosol Study (SOAS).

Site (Abbreviation)	Sampling Period
Jefferson Street (JST_May)	5/10/2012 - 6/2/2012
Yorkville (YRK_July)	6/26/2012 - 7/20/2012
Georgia Tech (GT_Aug)	7/20/2012 - 9/4/2012
Jefferson Street (JST_Nov)	11/6/2012 - 12/4/2012
Yorkville (YRK_Dec)	12/5/2012 - 1/10/2013
Roadside site (RS_Jan)	1/26/2013 - 2/28/2013
Centreville (CTR_June)	6/1/2013 – 7/15/2013

Table S2. Results of multivariate linear regression of the relationship between Isoprene-OA, particle water (H_2O_{ptcl}), particle acidity (H^+), and sulfate (SO_4^{2-}) by using total water (a) and organic water (b) for the Centreville data.

(a)

Variable	β-coefficient	Standard error	t Value	P value
Intercept	0.267	0.094	2.82	0.0049
[total-H_2O]	-0.004	0.008	-0.50	0.6171
$H^+_{(aq)}$	0.009	0.048	0.18	0.8540
[SO_4^{2-}]	0.424	0.022	19.23	<0.0001

(b)

Variable	β-coefficient	Standard error	t Value	P value
Intercept	0.172	0.095	1.81	0.0707
[Org-H_2O]	0.005	0.016	3.10	0.0020
$H^+_{(aq)}$	0.043	0.047	0.92	0.3599
[SO_4^{2-}]	0.396	0.018	22.32	<0.0001

579 Table S3. The campaign average nighttime concentration of VOCs in Centreville and their
580 reaction rate constants (29) used in the calculation of $NO_3^{\bullet}$ reactivity.

Species	Conc. (ppb)	reaction rate constant (cm^3 $molec^{-1}$ s^{-1})	$NO_3^{\bullet}$ reactivity (1/s)
propene	0.069	9.54E-15	1.60E-05
isoprene	1.917	6.96E-13	3.27E-02
propanal	0.080	6.31E-15	1.23E-05
methacrolein	0.385	3.40E-15	3.21E-05
n-butanal	0.024	1.10E-14	6.61E-06
ethylbenzene	0.008	1.50E-12	3.08E-04
m- and p-xylenes	0.019	3.80E-16	1.81E-07
o-xylene	0.009	3.80E-16	8.01E-08
α-pinene	0.350	6.21E-12	5.34E-02
camphene	0.058	2.51E-12	3.56E-03
1-ethyl-3- and 4-methylbenzene	0.035	6.60E-16	5.66E-07
β-pinene	0.312	2.51E-12	1.92E-02
1,3,5-trimethylbenzene	0.007	8.80E-16	1.59E-07
myrcene	0.009	1.28E-11	2.72E-03
1,2-dimethyl-4-ethylbenzene	0.007	1.80E-15	3.23E-07
limonene	0.050	1.22E-11	1.48E-02
p-cymene	0.021	9.90E-16	5.01E-07

581

582

583

584

585

586

587

588

589

590

591

592

Table S4: Estimated reaction branching ratio of isoprene, α-pinene, and β-pinene with respect to different oxidants for the Centreville data.

Species	Conc.[a] (ppb)	Rate Constant (cm^3 $molec^{-1}$ s^{-1})[b]		Branching Ratio	
		$NO_3^{\bullet}$	O_3	$NO_3^{\bullet}$	O_3
Isoprene	1.92	6.96E-13	1.27E-17	0.167	0.833
α-pinene	0.35	6.21E-12	9.00E-17	0.202	0.798
β-pinene	0.32	2.51E-12	1.50E-17	0.380	0.620

[a] Campaign average nighttime (20:00-5:00 local time) concentration in Centreville.

[b] Rate constants are from the Master Chemical Mechanism (http://mcm.leeds.ac.uk/MCM/) under 25°C, which is typical nighttime temperature in Centreville.

Table S5: Estimated nighttime SOA production from isoprene, α-pinene, and β-pinene from various oxidation pathways in Centreville.

Species	SOA yield from literature*		[SOA] (μg m^{-3})	
	$NO_3^{\bullet}$	O_3	$NO_3^{\bullet}$	O_3
Isoprene	0.10†	0‡	0.089	0.000
α-pinene	0.007¶	0.15‖	0.003	0.232
β-pinene	0.55**	0.03††	0.371	0.033

* SOA yields at mass loadings relevant to Centreville (i.e., ~8 μg m^{-3})

† Ng et al. 2008 (Expt on 8/14/07 in Table 1) (35)

‡ Kleindienst et al. 2007 (36)

¶ Hallquist et al. 1999 (18ppb initial α-pinene in Table 1) (37)

‖ Shilling et al. 2008 (Estimate from Fig. 3) (38)

**Results from laboratory chamber experiments conducted in the current study.

††Griffin et al. 1999 (Expt 6/11/98a in Table 2b) (39)

Fig. S1: Diurnal trends of temperature (bottom plot), relative humidity (RH, middle plot), and boundary layer height (BLH, top plot) for the Centreville data. The upper and lower boundaries of the shaded area represent 75 and 25 percentiles. The line within the shaded area marks the median value.

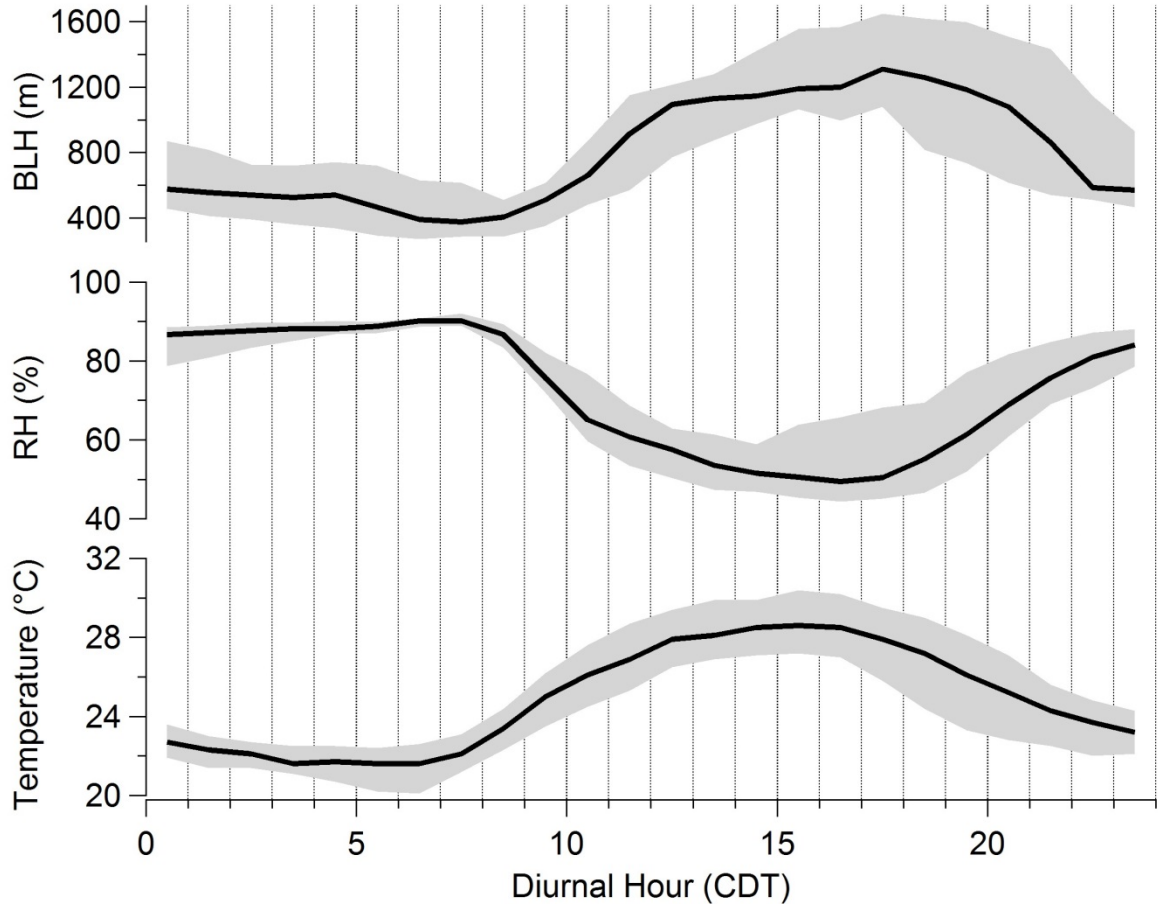

Fig. S2: Time series (a) and diurnal trend (b) of organics (OA), sulfate (SO_4^{2-}), nitrate (NO_3^-), ammonium (NH_4^+), and chloride (Cl^-) as measured by HR-ToF-AMS in Centreville. Inset of (a) shows the campaign average composition. Panel (c) shows the normalized mass spectrum of OA (colored by ion type). The median values are reported in the diurnal trends.

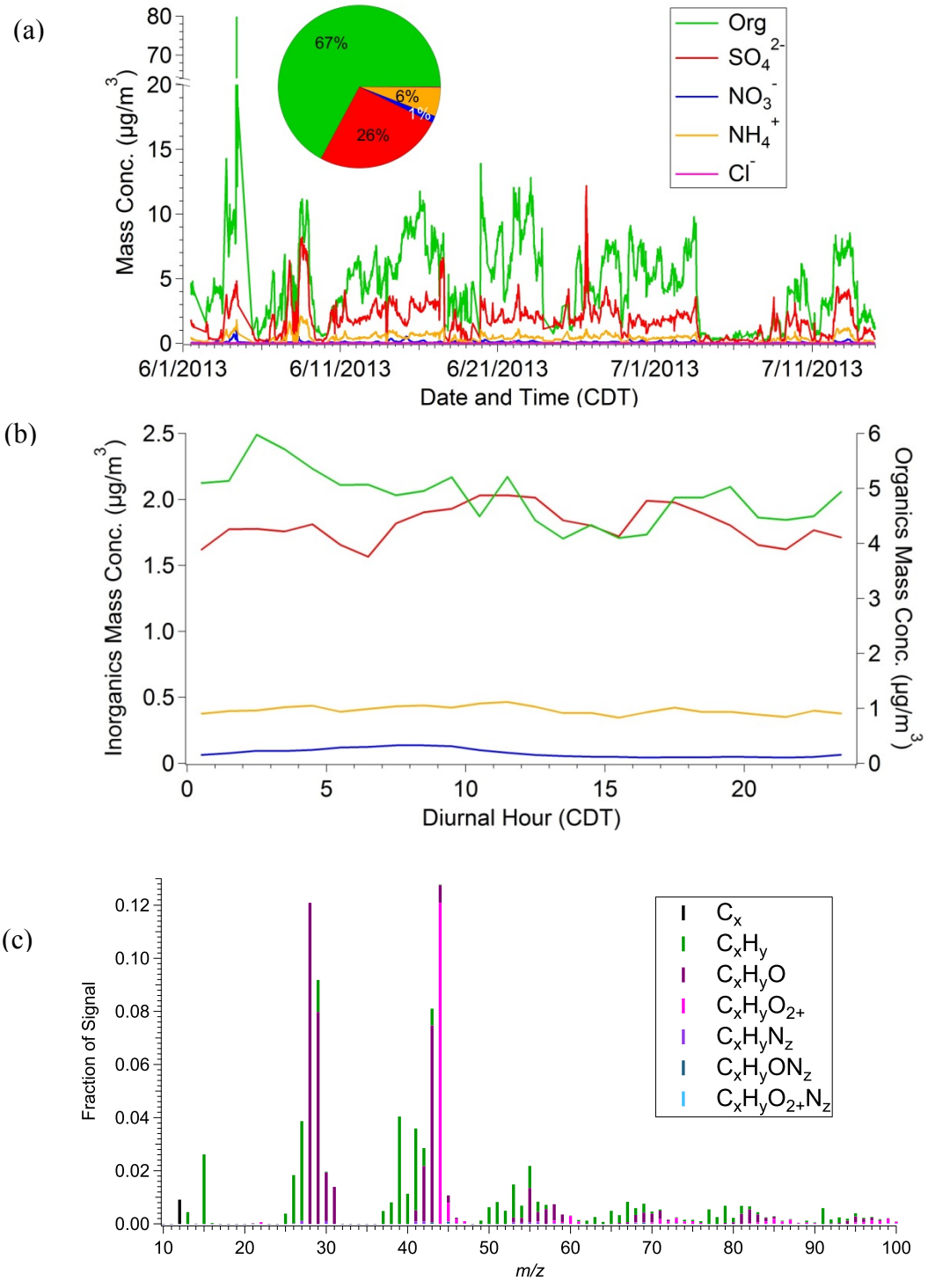

Fig. S3. Summary of key diagnostic plots of the PMF results for the Centreville data. (a) Q/Q_{exp} as a function of number of factors. (b) Q/Q_{exp} as a function of FPEAK for the 4-factor solution. (c) Mass fraction of PMF factors as a function of FPEAK. (d) Correlations of time series and mass spectra among PMF factors. (e) The distribution of scaled residuals for each *m/z*. The boxes represent ±25% of points. (f) Time series of the measured and the reconstructed organic mass. (g) Variations of the residual (= measured - reconstructed) of the least-square-fit as a function of time. (h) The Q/Q_{exp} for each point as a function of time. (i) The Q/Q_{exp} values for each *m/z*.

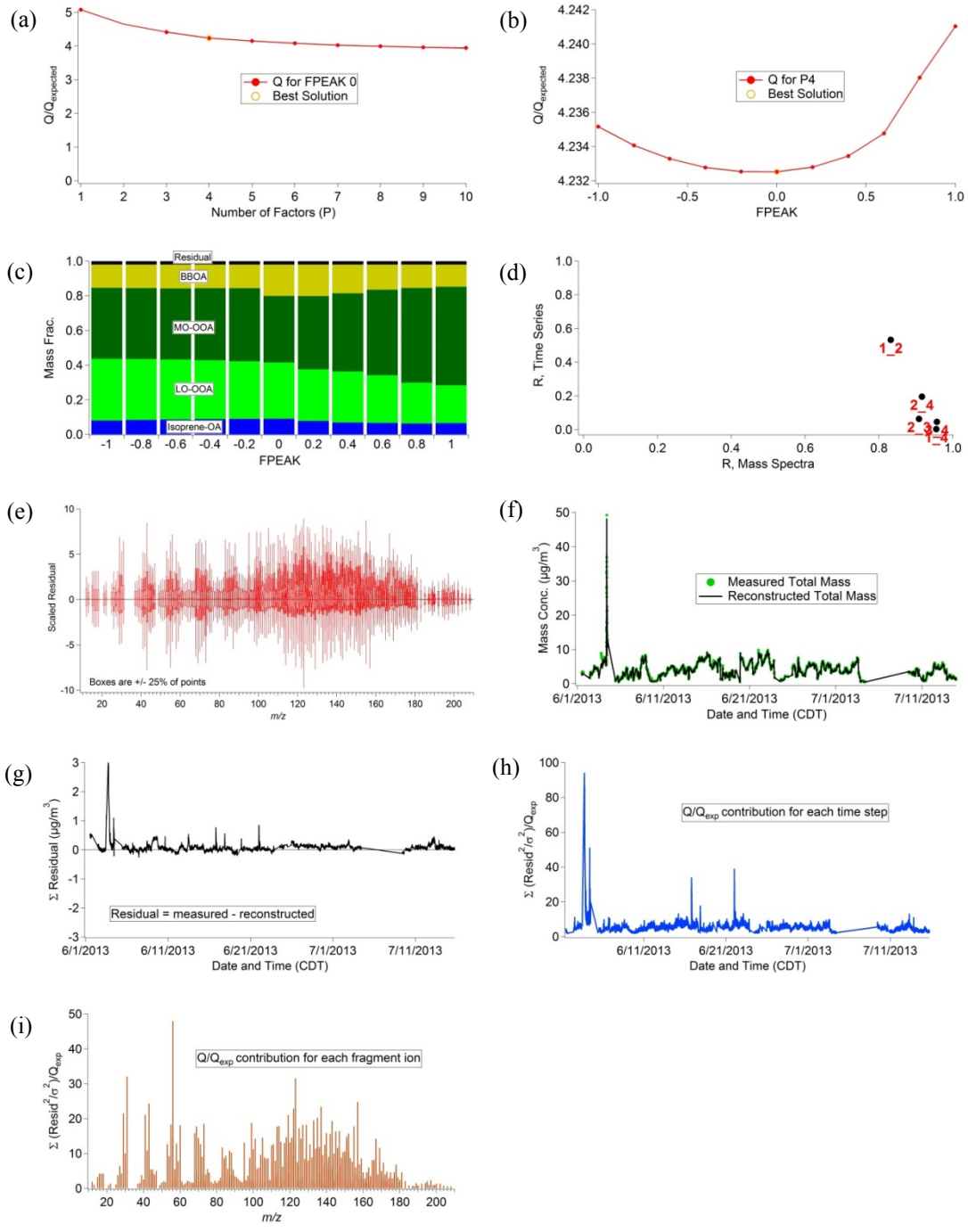

Fig. S4. The diurnal trends of isoprene, α-pinene, β-pinene, Isoprene-OA, and LO-OOA factor for the Centreville data. The median values are reported.

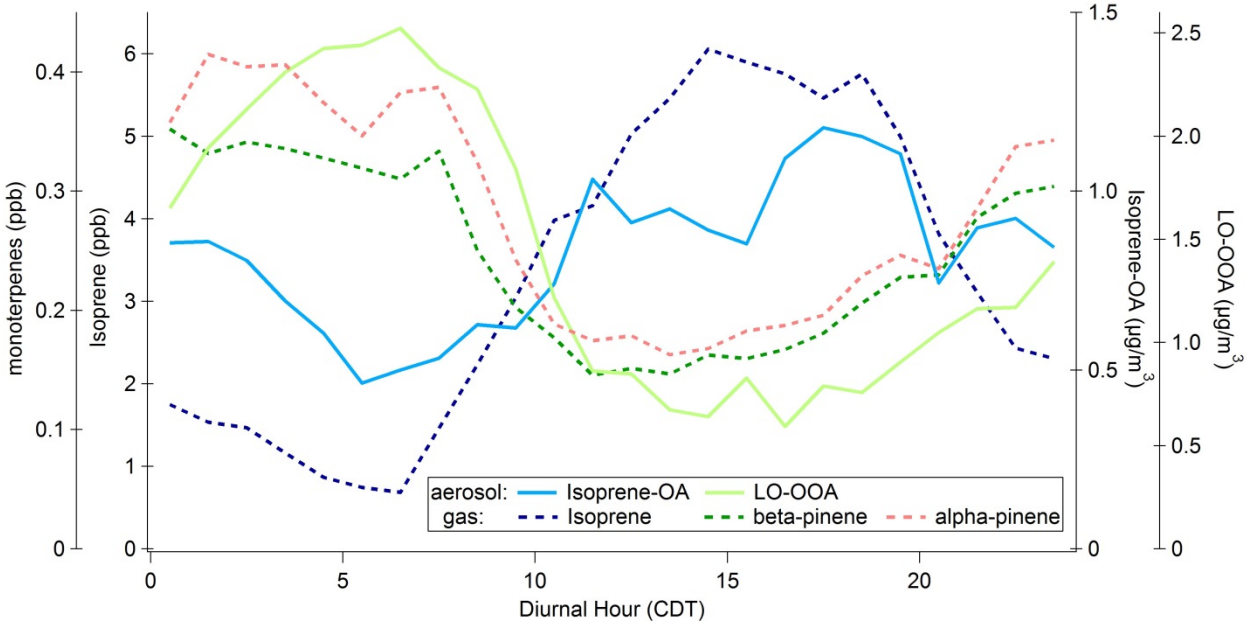

Fig. S5. The time series of Isoprene-OA, LO-OOA, MO-OOA, and sulfate (SO_4^{2-}) in Yorkville July, 2012. Isoprene-OA correlates well with SO_4^{2-} (R=0.85). The black box indicates the period when sulfate concentration decreased dramatically (from 22:30 July 5 to 16:30 July 6).

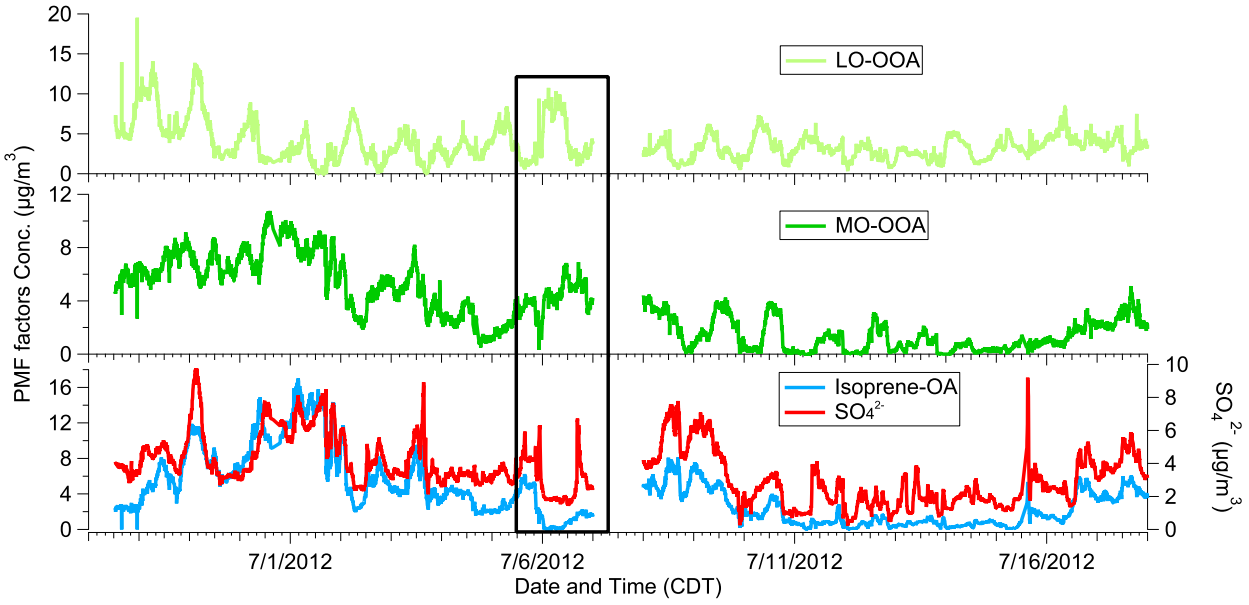

Fig. S6. Relationship between particle water (H_2O_{ptcl}), particle acidity (H^+), sulfate (SO_4^{2-}), and Isoprene-OA for Centreville (a) and three SCAPE datasets (b, c, d), where isoprene-OA factor is resolved. For Centreville, data points are colored by gas-phase [NH_3], which is measured by Chemical Ionization Mass Spectrometer (CIMS).

(a) Centreville

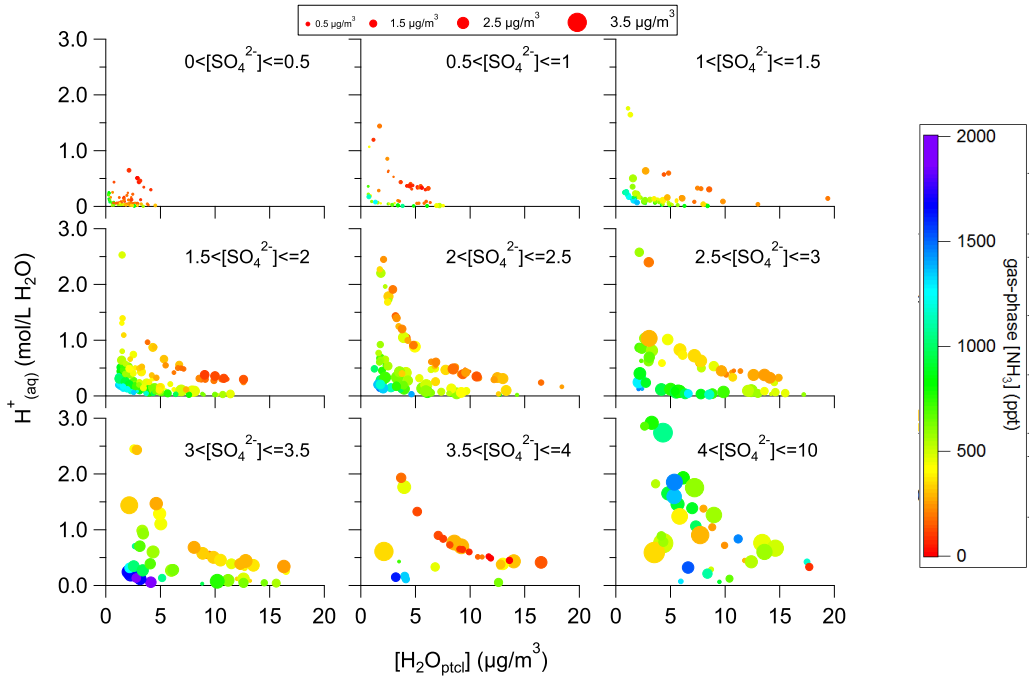

(b) Jefferson Street (JST_May)

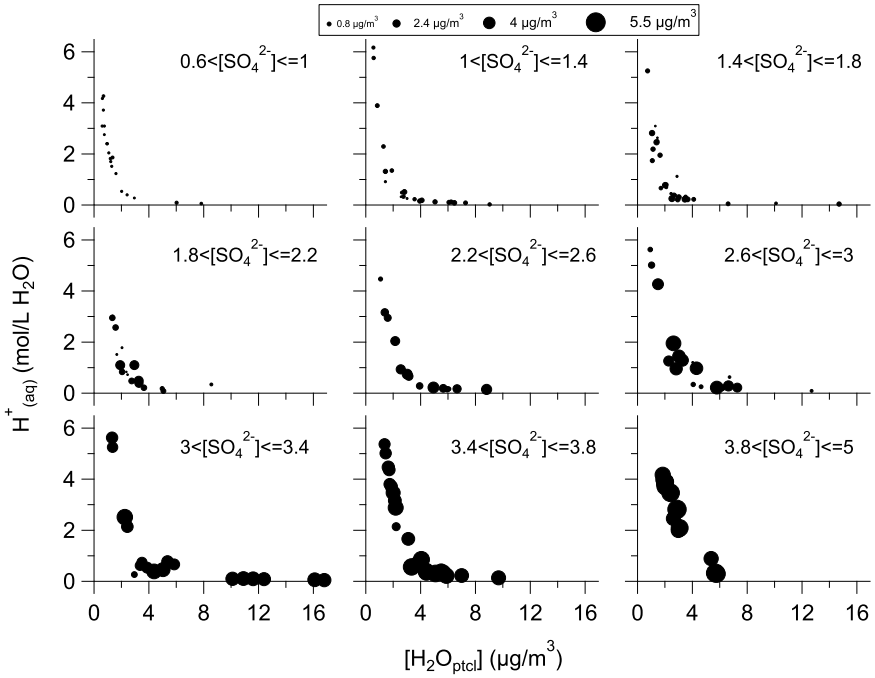

(c) Yorkville (YRK_July)

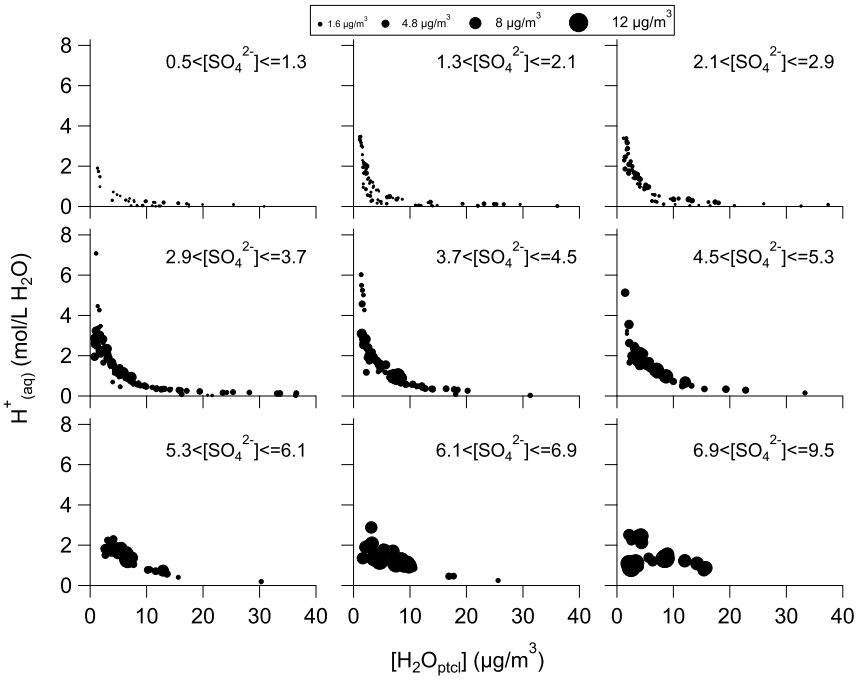

(d) Georgia Tech (GT_Aug)

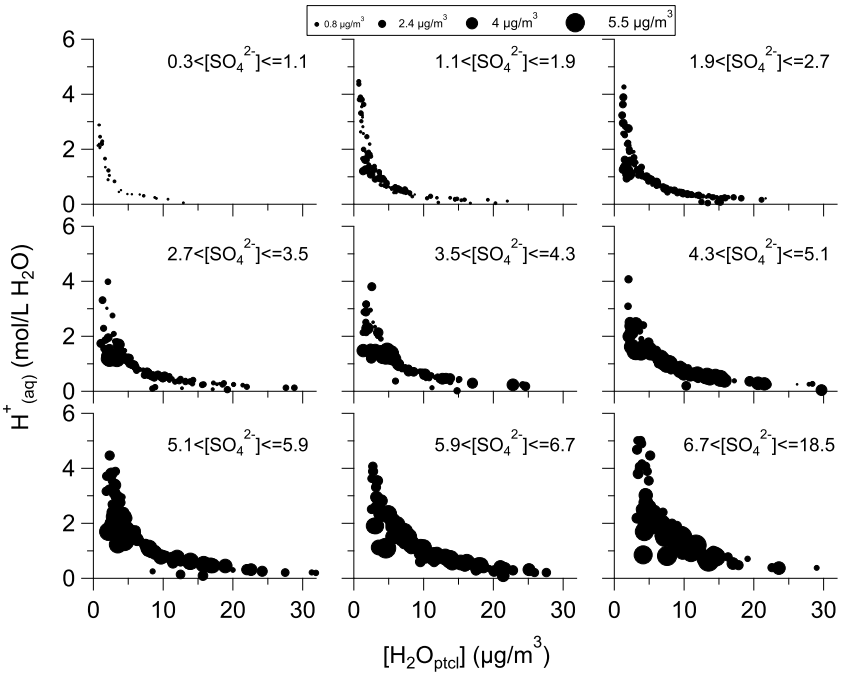

Fig. S7. Diurnal trends of H_2O_{ptcl} mass concentration (µg m^{-3} air) and the aqueous phase SO_4^{2-} concentration (mol L^{-1} H_2O) in Centreville. The upper and lower boundaries of the shaded area represent 75 and 25 percentiles. The line within the shaded area marks the median value.

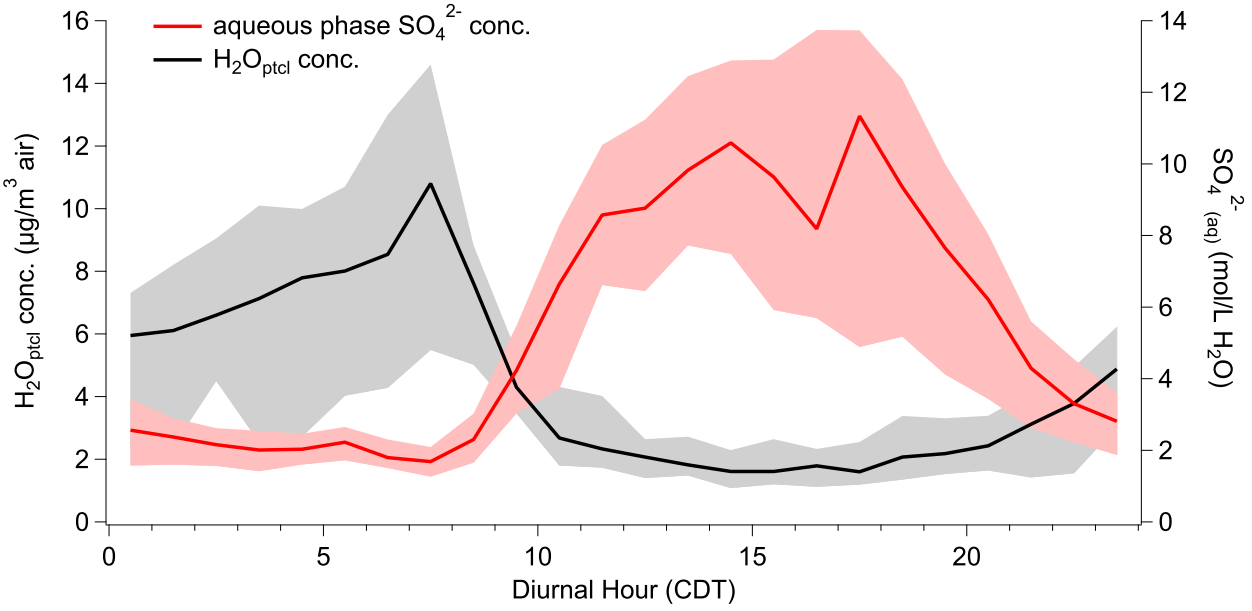

731 Fig. S8. The diurnal trends of the LO-OOA factor for Centreville and all SCAPE datasets. The
732 diurnal trends are normalized by the highest LO-OOA concentration of each dataset.
733 Abbreviations correspond to Centreville (CTR), Yorkville (YRK), Jefferson Street (JST),
734 Georgia Institute of Technology (GT), and Roadside (RS).

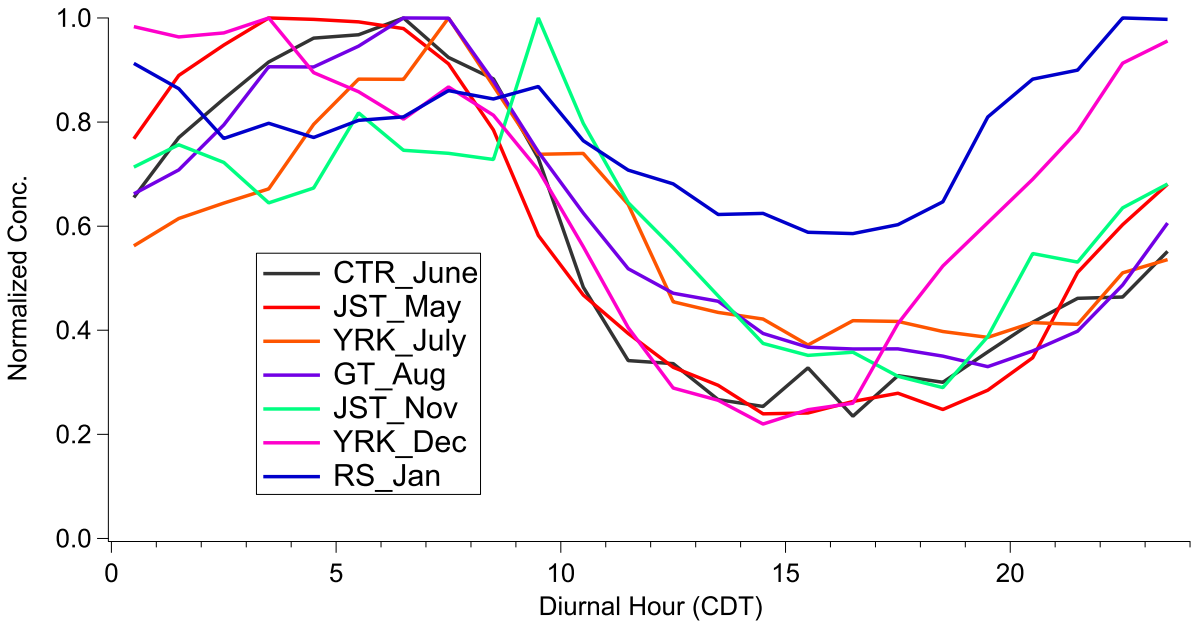

735

736

Fig. S9. Source regions of air masses sampled in Centreville during the SOAS campaign. Shown are residence times calculated by FLEXPART, integrated vertically and over the duration of the campaign (2013-06-01 00:00 to 2013-07-14 21:00 UTC time). Particles (representing an inert tracer only affected by advection, turbulence and convection) were released in Centreville every 3 hours and followed back in time for 72 hours. Areas delineated by dashed lines (NE, NW, SE, SW) indicate the regions used in determining air mass origin.

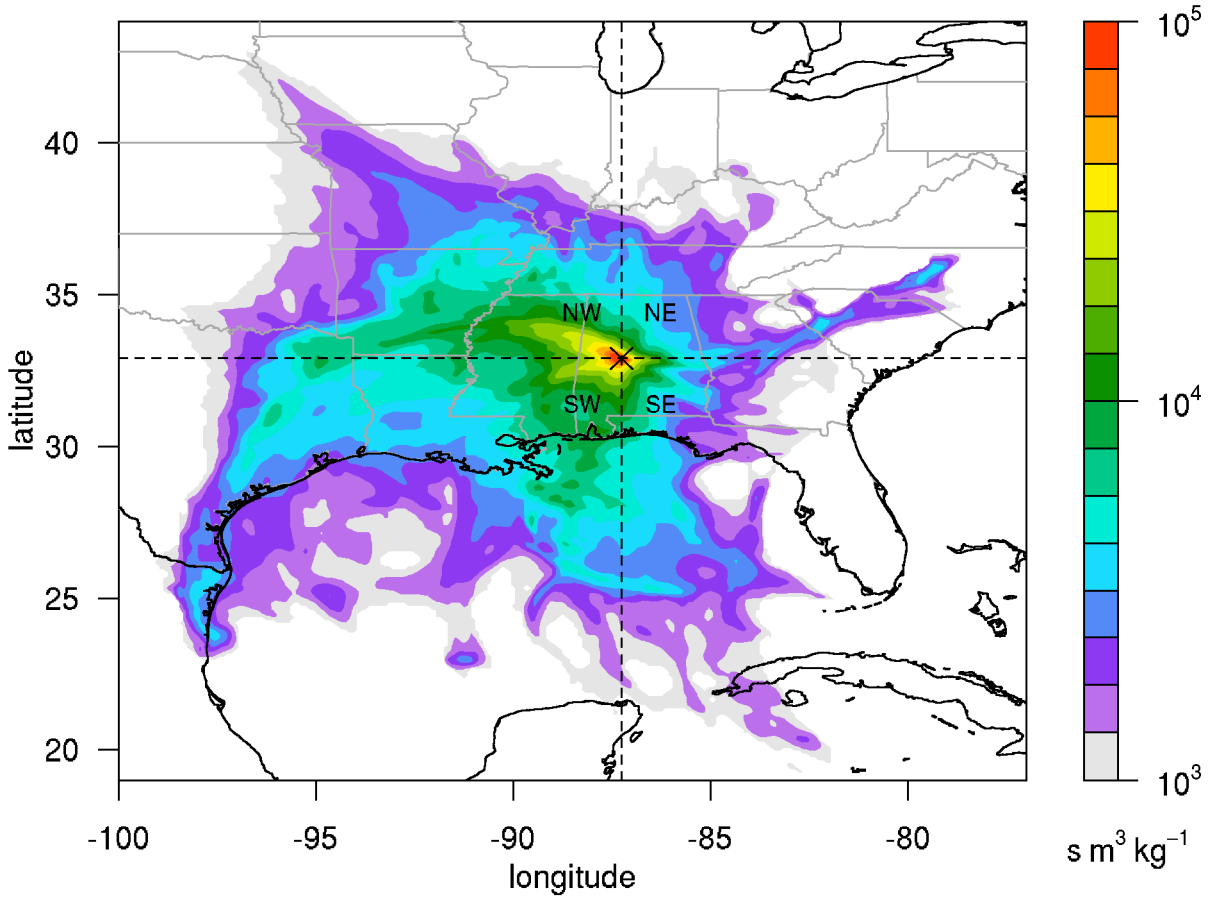

Fig. S10. (a) Frequency of air masses origin as a function of diurnal hour at Centreville. Abbreviations correspond to Northwest (NW), Northeast (NE), Southwest (SW), and Southeast (SE). (b) Grouped diurnal trend of LO-OOA (b) and Isoprene-OA (c) based on the origins of air masses. The upper and lower boundaries of the shaded area represent 75 and 25 percentiles. The line within the shaded area marks the median value.

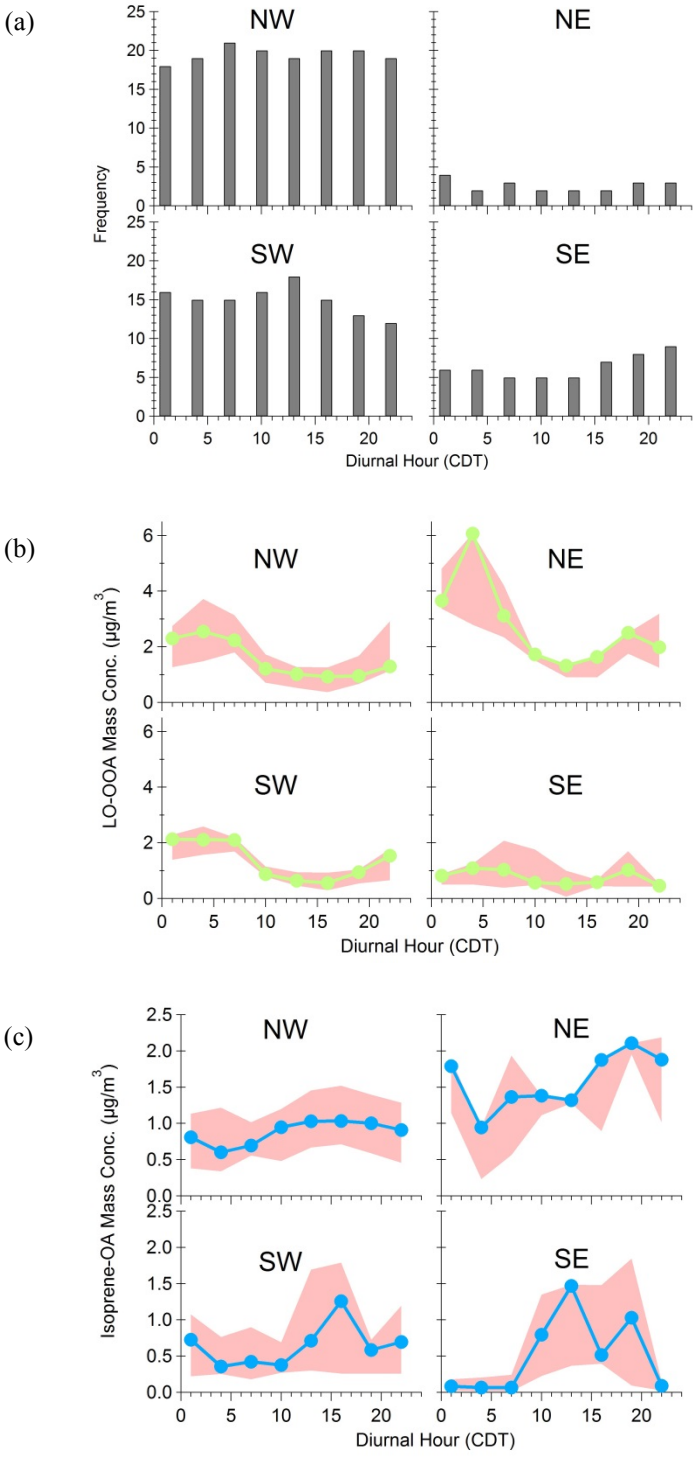

Fig. S11. Estimated contribution of organic nitrates to LO-OOA.

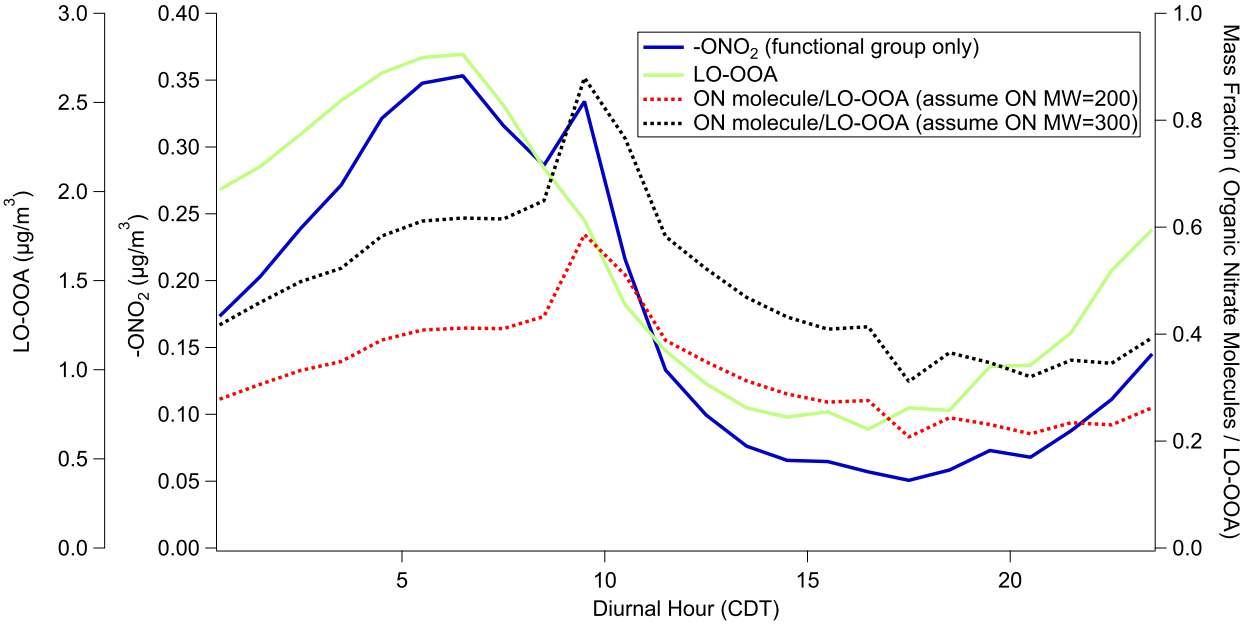

Fig. S12. Estimated nighttime contribution to LO-OOA through different oxidation pathways and different SOA precursors in Centreville.

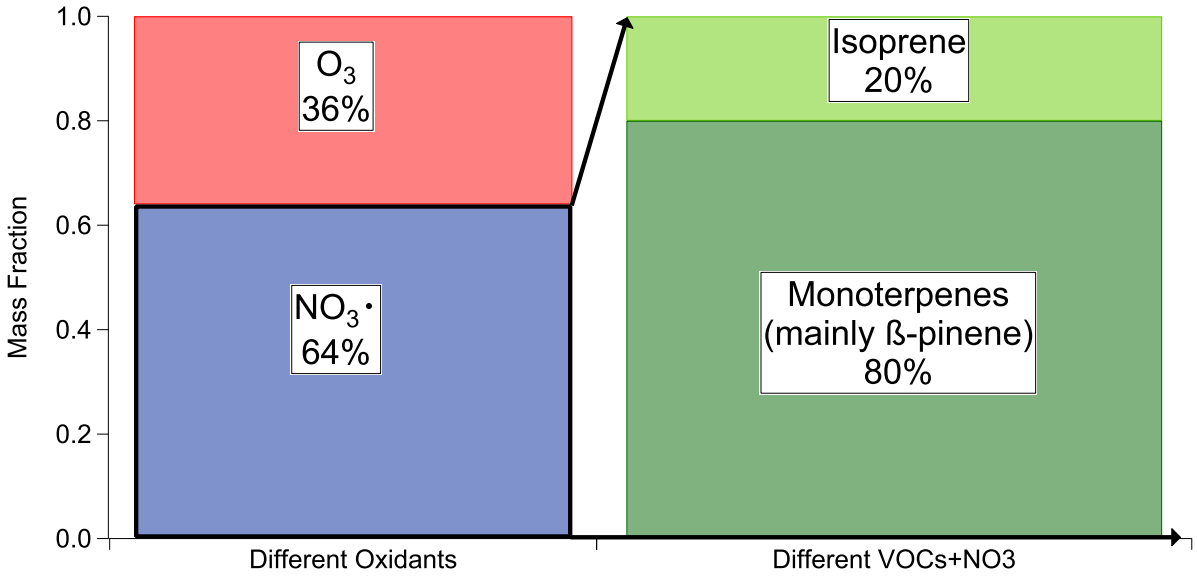

784 Fig S13: Seasonal variation of correlation coefficient (R) between OC and sulfate at Centreville
785 site from 2006 to 2010.

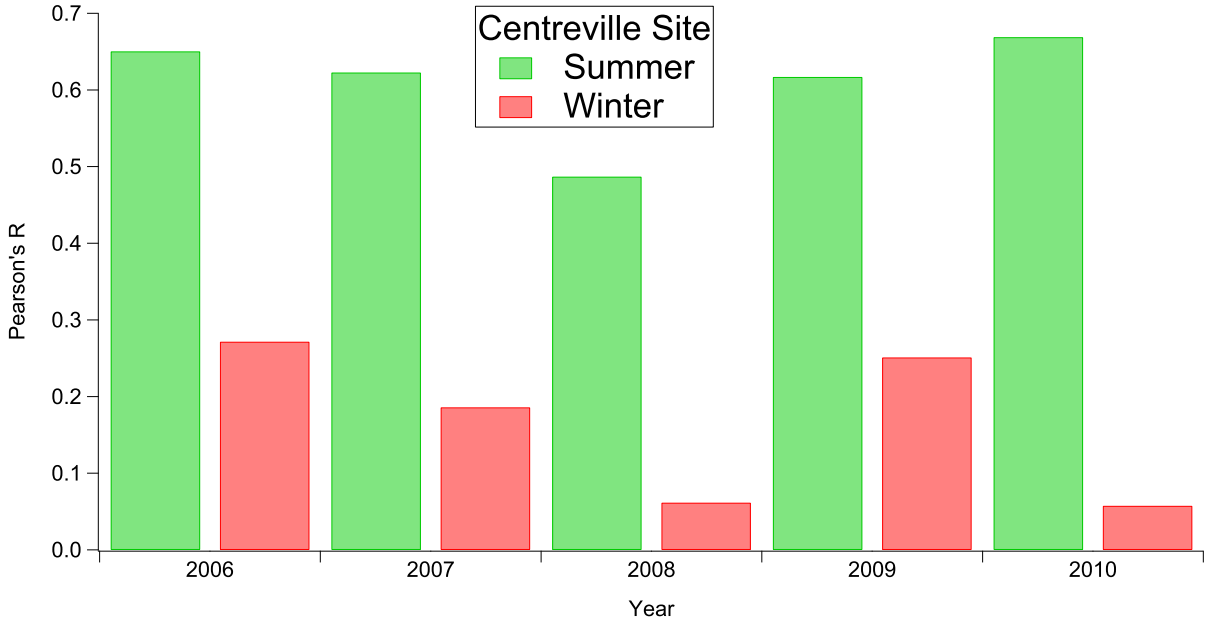

786

787

788

789